# Universal collaborative couplings between oxygen-octahedral rotations and antiferroelectric distortions in perovskites

L. Bellaiche[1] and Jorge Íñiguez[2]

[1]*Physics Department and Institute for Nanoscience and Engineering, University of Arkansas, Fayetteville, Arkansas 72701, USA*

[2]*Institut de Ciència de Materials de Barcelona (ICMAB-CSIC), Campus UAB, 08193 Bellaterra, Spain*

(Received 4 April 2013; revised manuscript received 9 June 2013; published 11 July 2013)

We identify two elemental interatomic couplings that control the collaborative (as opposed to competing) interaction between the $O_6$ octahedral rotations (usually called antiferrodistortive or AFD modes) and the antiferroelectric (AFE) displacement patterns of the *A*-site cations in oxides with the $ABO_3$ perovskite structure. Straightforward analytical derivations allow us to reproduce and explain the origin of various long-range AFE orders that have been previously found in different phases of several perovskite compounds, all possessing simple or even complex long-range AFD patterns. Our analysis also leads to the prediction of original peculiar combinations of AFD and AFE orders that are awaiting to be observed.

DOI: 10.1103/PhysRevB.88.014104 PACS number(s): 77.80.−e, 61.50.Ah, 61.68.+n

## I. INTRODUCTION

Many $ABO_3$ perovskite materials display concerted oxygen octahedral tiltings usually termed antiferrodistortive (AFD) modes (see, e.g., Refs. 1–7 and references therein). Typically, the AFD modes *compete* with ferroelectric (FE) distortions,[8] and such a competition may have drastic consequences on the macroscopic materials properties. For example, first-principles-based model theories of $PbZr_{1-x}Ti_xO_3$[2] and $PbTiO_3$[9] revealed that the AFD-FE competition results in a drastic reduction of the Curie temperature of these compounds. Similarly, the fact that the Curie temperature of some epitaxial ferroelectric and multiferroic thin films (under short-circuit-like boundary conditions) adopts a counterintuitive behavior, decreasing for a growing compressive strain,[10,11] is also a manifestation of the competitive nature of the coupling between the AFD and FE instabilities. Another consequence is the fact that AFD and FE motions do *not* spatially coexist in domains occurring in some FE films under open-circuit-like boundary conditions: the oxygen octahedral tiltings are found to be large near the domain walls while the FE distortions are significant only *inside* the "up" and "down" domains.[12,13]

Interestingly, perovskite compounds can also be *antiferroelectric* (AFE) rather than ferroelectric,[14,15] and AFE materials are gaining renewed attention due to their prospective applications in the field of energy.[16,17] Remarkably, different AFD patterns were recently found to *coexist* with AFE distortions in several $ABO_3$ perovskites, with a precise correlation existing between the type of tilting pattern and the kind of antipolar movements of the *A*-site cations (see, e.g., Refs. 18–22 and references therein). Moreover, in some cases, it has been shown from first principles that the AFE pattern plays a key role in the stabilization of specific AFD motions.[19,22] One may thus wonder if it is a general behavior that the AFD and AFE motions, unlike AFD and FE degrees of freedom, in fact, *collaborate* rather than compete. Further, we may ask ourselves whether, intrinsic to the perovskite structures, there may be *universal* interatomic couplings that govern such a collaboration and determine the specific AFD-AFE combinations that can occur. Note that such hypothetical interatomic couplings should be allowed by symmetry in any perovskite (hence their *universal* character) and automatically guarantee a *collaborative* coupling between AFD and AFE variables.

The aim of this article is to demonstrate the existence, and provide the analytical forms, of such coupling energy terms. As we will see, these elemental terms naturally reproduce *all* the peculiar AFE patterns that have been recently found to be associated with specific AFD distortions. From these terms, we also predict peculiar combinations of AFD and AFE patterns that, to the best of our knowledge, have yet to be discovered.

The article is organized as follows. Section II provides the analytical expressions for the atomistic energy terms that locally couple AFD motions and cation displacements in a collaborative fashion, and also describes the derivation of some useful formula. In Sec. III, these formula are applied to the case of simple and complex AFD patterns to predict the induced AFE configurations. Finally, Sec. IV summarizes this work and emphasizes its consequences for both experimentalists and theorists working on properties of perovskites. Let us note here that the precise definition of an AFE material, and the distinction between AFE and antipolar displacement patterns, is currently generating some debate.[17] In this article, we use the terms antiferroelectric and antipolar indifferently.

## II. FORMALISM

Let us start by defining the local AFD mode $\boldsymbol{\omega}_i$ that characterizes the tilting of the oxygen octahedron centered at the *B* site in unit cell $i$. (Here, we adopt the convention that the *B* cations are at the corners of the reference five-atom cell, and the *A* cations are at the cell center.) As sketched in Fig. 1, the direction of this pseudovector provides the axis about which the oxygen octahedron rotates and its magnitude yields the rotation angle.[2] Thus, for instance, $\boldsymbol{\omega}_i = 0.1(\mathbf{x}+\mathbf{y}+\mathbf{z})$ corresponds to a rotation by $0.1\sqrt{3}$ radians about the [111] axis, with $\mathbf{x}$, $\mathbf{y}$, and $\mathbf{z}$ denoting the unit vectors along the [100], [010], and [001] pseudocubic directions, respectively. Moreover, $\boldsymbol{\omega}_{ilmn}$ will represent rotation of the $O_6$ group in the cell that is reached from $i$ by following the lattice vector $\mathbf{R}_{lmn} = a_{\text{lat}}(l\mathbf{x}+m\mathbf{y}+n\mathbf{z})$, where $a_{\text{lat}}$ is the lattice constant of the five-atom cubic cell and $l$, $m$, and $n$ are integers.

Also sketched in Fig. 1 is the vector $\mathbf{u}_i$ giving the off-centering displacement of the *A*-site cation at cell $i$. Note that

 

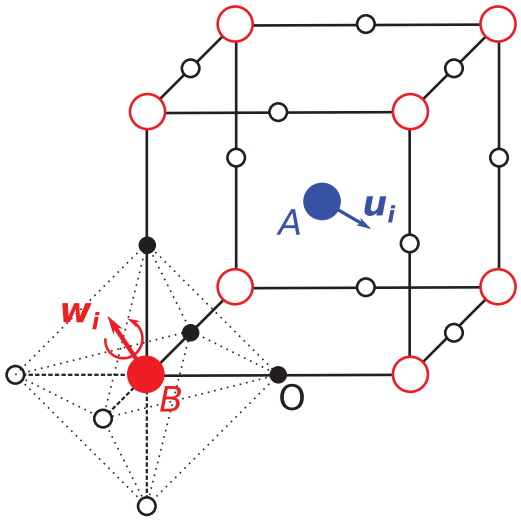


FIG. 1. (Color online) Sketch of the elemental five-atom perovskite cell, with the $A$ site (blue circle) at the cell center and the $B$ sites (red circles) at the corners. Oxygens represented by small black circles are at the mid points of the cell edges. The atoms within the unit cell are represented by solid symbols; open symbols represent periodic images. The $A$-cation polar distortion ($\mathbf{u}_i$) and $B$-centered oxygen octahedra rotation ($\boldsymbol{\omega}_i$) associated to this $i$th cell are pictorially indicated.

these vectors can give rise to both FE and AFE displacement patterns, depending on how they correlate from cell to cell.

Now, we want to investigate whether an AFD motion can induce the displacement of (or, equivalently, cause a force acting on) the $A$ cations. Figure 2 illustrates two simple and representative situations: (a) shows how the 12 oxygen atoms neighboring a specific $A$ cation displace according to a simple AFD pattern. In particular, we present the concerted rotation of $O_6$ groups that is denoted as $a^-a^-a^-$ in the well-known notation introduced by Glazer,[1] i.e., we have $\boldsymbol{\omega}_0 = \omega(1,1,1)$ for the $O_6$ group in the cell at the origin and an antiphase modulation of the rotations as we move to neighboring cells along any of the principal cubic directions. Interestingly, these equal-amplitude rotations about the three peudocubic axes do change the first oxygen-coordination shell of the $A$ cation in Fig. 2(a), but do not induce any force on it. To understand this, one can for example look at the three oxygens that come closer to the $A$ cation upon the condensation of the $a^-a^-a^-$ distortion, which are marked with asterisks in the figure; these closest anions form a very symmetric configuration around the $A$ atom, and induce no net force on it. On the other hand, panel (b) shows a different AFD pattern denoted as $a^-a^-c^+$ in Glazer's notation (i.e., we have equal-amplitude rotations modulated in antiphase about the $x$ and $y$ axes and a third in-phase rotational distortion about $z$).

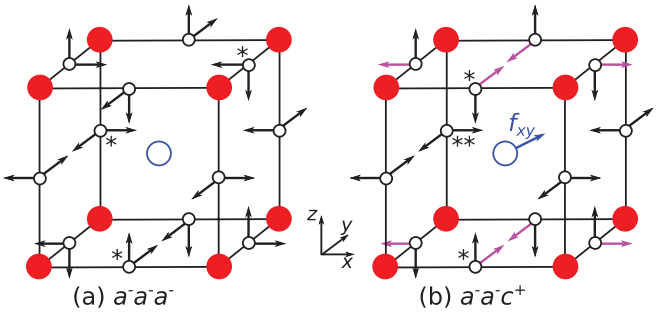


FIG. 2. (Color online) Schematic representation of two simple AFD patterns, indicating with arrows the displacements affecting the oxygen atoms. The oxygens that get closest to the central $A$ cation are marked with asterisks; in (b), there are two symmetry-inequivalent cases, marked with single and double asterisks, respectively.

Here again, there are three oxygens that get the closest to the $A$ cation and which are marked with asterisks in Fig. 2(b); however, in this case the closest oxygens form a low-symmetry first coordination shell, and it is clear that the $A$ cation must feel some sort of forces along the $x$ and $y$ directions. This will result in an $A$-site off-centering accompanying the $a^-a^-c^+$ pattern.

We thus tried to find energetic terms that are associated with the forces appearing on the $A$ cations when their 12 neighboring oxygens distort and break symmetry as a result of $O_6$ rotations. We adopted the effective-Hamiltonian type of approach to structural transitions in perovskite oxides,[21,23] which relies on a Taylor-series expansion of the materials energy around its natural reference configuration (i.e., the cubic perovskite prototype phase) as a function of the relevant degrees of freedom. In our case, such degrees of freedom are the $O_6$ rotations $\boldsymbol{\omega}_i$ and the off-centering $A$-cation displacements $\mathbf{u}_i$. Thus we set up to identify the lowest-order $\omega$-$u$ couplings satisfying the following conditions: (i) linearity in $\mathbf{u}_i$, as required to generate forces on the $A$ cations and (ii) nonzero contribution to the energy for *simple* rotational patterns that can be expressed in Glazer's notation (i.e., those involving concerted $O_6$ rotations modulated exactly in phase or in antiphase and a small repetition period). Regarding condition ($i$), note that the interactions of interest will result in AFD-induced forces on the $A$ cations *irrespective* of the sign of the associated coupling parameter; in other words, by construction these couplings are always *collaborative*. Regarding condition (ii), note that this is sufficient to investigate the cases sketched in Fig. 2, which are representative of the rhombohedral ($a^-a^-a^-$) and orthorhombic ($a^-a^-c^+$) structures displayed by most perovskite oxides.

Our analysis led us to identify the following two terms, which we will denote as $\Delta E_1$ and $\Delta E_2$:

$$\begin{aligned}\Delta E_1 = K_1 \sum_i [&u_{i,z}(\omega_{i,y}\omega_{i,z} + \omega_{i100,y}\omega_{i100,z} + \omega_{i001,y}\omega_{i001,z} + \omega_{i101,y}\omega_{i101,z}) \\ &- u_{i,z}(\omega_{i110,y}\omega_{i110,z} + \omega_{i010,y}\omega_{i010,z} + \omega_{i011,y}\omega_{i011,z} + \omega_{i111,y}\omega_{i111,z}) \\ &+ u_{i,z}(\omega_{i,x}\omega_{i,z} + \omega_{i010,x}\omega_{i010,z} + \omega_{i001,x}\omega_{i001,z} + \omega_{i011,x}\omega_{i011,z}) \\ &- u_{i,z}(\omega_{i100,x}\omega_{i100,z} + \omega_{i110,x}\omega_{i110,z} + \omega_{i101,x}\omega_{i101,z} + \omega_{i111,x}\omega_{i111,z})\end{aligned}$$

$$
\begin{aligned}
&+u_{i,x}(\omega_{i,x}\omega_{i,z}+\omega_{i010,x}\omega_{i010,z}+\omega_{i100,x}\omega_{i100,z}+\omega_{i110,x}\omega_{i110,z})\\
&-u_{i,x}(\omega_{i011,x}\omega_{i011,z}+\omega_{i001,x}\omega_{i001,z}+\omega_{i101,x}\omega_{i101,z}+\omega_{i111,x}\omega_{i111,z})\\
&+u_{i,x}(\omega_{i,x}\omega_{i,y}+\omega_{i001,x}\omega_{i001,y}+\omega_{i100,x}\omega_{i100,y}+\omega_{i101,x}\omega_{i101,y})\\
&-u_{i,x}(\omega_{i010,x}\omega_{i010,y}+\omega_{i011,x}\omega_{i011,y}+\omega_{i110,x}\omega_{i110,y}+\omega_{i111,x}\omega_{i111,y})\\
&+u_{i,y}(\omega_{i,x}\omega_{i,y}+\omega_{i001,x}\omega_{i001,y}+\omega_{i010,x}\omega_{i010,y}+\omega_{i011,x}\omega_{i011,y})\\
&-u_{i,y}(\omega_{i101,x}\omega_{i101,y}+\omega_{i100,x}\omega_{i100,y}+\omega_{i110,x}\omega_{i110,y}+\omega_{i111,x}\omega_{i111,y})\\
&+u_{i,y}(\omega_{i,z}\omega_{i,y}+\omega_{i100,z}\omega_{i100,y}+\omega_{i010,z}\omega_{i010,y}+\omega_{i110,z}\omega_{i110,y})\\
&-u_{i,y}(\omega_{i001,z}\omega_{i001,y}+\omega_{i101,z}\omega_{i101,y}+\omega_{i011,z}\omega_{i011,y}+\omega_{i111,z}\omega_{i111,y})]
\end{aligned}
\tag{1}
$$

and

$$
\begin{aligned}
\Delta E_2 = K_2\sum_i\big[&u_{i,z}\big(\omega^2_{i100,y}\omega_{i100,z}+\omega^2_{i001,y}\omega_{i001,z}+\omega^2_{i010,y}\omega_{i010,z}+\omega^2_{i111,y}\omega_{i111,z}\big)\\
&-u_{i,z}\big(\omega^2_{i,y}\omega_{i,z}+\omega^2_{i101,y}\omega_{i101,z}+\omega^2_{i110,y}\omega_{i110,z}+\omega^2_{i011,y}\omega_{i011,z}\big)\\
&+u_{i,z}\big(\omega^2_{i,x}\omega_{i,z}+\omega^2_{i011,x}\omega_{i011,z}+\omega^2_{i110,x}\omega_{i110,z}+\omega^2_{i101,x}\omega_{i101,z}\big)\\
&-u_{i,z}\big(\omega^2_{i010,x}\omega_{i010,z}+\omega^2_{i001,x}\omega_{i001,z}+\omega^2_{i100,x}\omega_{i100,z}+\omega^2_{i111,x}\omega_{i111,z}\big)\\
&+u_{i,x}\big(\omega_{i010,x}\omega^2_{i010,z}+\omega_{i100,x}\omega^2_{i100,z}+\omega_{i001,x}\omega^2_{i001,z}+\omega_{i111,x}\omega^2_{i111,z}\big)\\
&-u_{i,x}\big(\omega_{i,x}\omega^2_{i,z}+\omega_{i110,x}\omega^2_{i110,z}+\omega_{i011,x}\omega^2_{i011,z}+\omega_{i101,x}\omega^2_{i101,z}\big)\\
&+u_{i,x}\big(\omega_{i,x}\omega^2_{i,y}+\omega_{i101,x}\omega^2_{i101,y}+\omega_{i011,x}\omega^2_{i011,y}+\omega_{i110,x}\omega^2_{i110,y}\big)\\
&-u_{i,x}\big(\omega_{i001,x}\omega^2_{i001,y}+\omega_{i100,x}\omega^2_{i100,y}+\omega_{i010,x}\omega^2_{i010,y}+\omega_{i111,x}\omega^2_{i111,y}\big)\\
&+u_{i,y}\big(\omega^2_{i001,x}\omega_{i001,y}+\omega^2_{i010,x}\omega_{i010,y}+\omega^2_{i100,x}\omega_{i100,y}+\omega^2_{i111,x}\omega_{i111,y}\big)\\
&-u_{i,y}\big(\omega^2_{i,x}\omega_{i,y}+\omega^2_{i011,x}\omega_{i011,y}+\omega^2_{i101,x}\omega_{i101,y}+\omega^2_{i110,x}\omega_{i110,y}\big)\\
&+u_{i,y}\big(\omega^2_{i,z}\omega_{i,y}+\omega^2_{i110,z}\omega_{i110,y}+\omega^2_{i101,z}\omega_{i101,y}+\omega^2_{i011,z}\omega_{i011,y}\big)\\
&-u_{i,y}\big(\omega^2_{i100,z}\omega_{i100,y}+\omega^2_{i010,z}\omega_{i010,y}+\omega^2_{i001,z}\omega_{i001,y}+\omega^2_{i111,z}\omega_{i111,y}\big)\big],
\end{aligned}
\tag{2}
$$

where the sum over $i$ runs over all the cells of the perovskite structure; the $x$, $y$, and $z$ subscripts denote the Cartesian components of the $\mathbf{u}_i$ vectors and $\boldsymbol{\omega}_i$ pseudovectors. Figure 3 gives a graphical, more intuitive representation of these coupling terms.

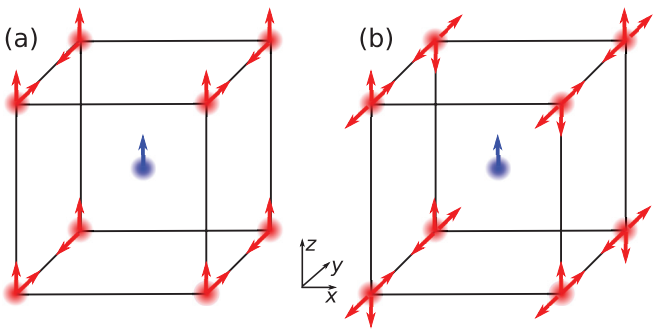


FIG. 3. (Color online) Sketch of representative coupling terms in (a) $\Delta E_1$ [see Eq. (1)] and (b) $\Delta E_2$ [see Eq. (2)]. In both cases, we sketch the first eight couplings appearing in the corresponding equation in the text. The blue arrow on the central $A$ cation stands for the $u_{i,z}$ displacement; the red arrows on the corner $B$ cations represent components of the $\boldsymbol{\omega}$ pseudovectors, with double arrows standing for squared components. The rest of terms in Eqs. (1) and (2) can be derived from the ones shown by application of the operations of the cubic $Pm\bar{3}m$ space group of the perovskite structure.

Let us now consider distortions of the form

$$
\begin{aligned}
\omega_{i,x} &= \tfrac{1}{2}A\,[\exp(i\mathbf{k}_x\cdot\mathbf{R}_i)+\text{c.c.}],\\
\omega_{i,y} &= \tfrac{1}{2}B\,[\exp(i\mathbf{k}_y\cdot\mathbf{R}_i)]+\text{c.c.}],\\
\omega_{i,z} &= \tfrac{1}{2}C\,[\exp(i\mathbf{k}_z\cdot\mathbf{R}_i)+\text{c.c.}],\\
u_{i,x} &= \tfrac{1}{2}A'\,[\exp(i\mathbf{k}'_x\cdot\mathbf{R}_i)+\text{c.c.}],\\
u_{i,y} &= \tfrac{1}{2}B'\,[\exp(i\mathbf{k}'_y\cdot\mathbf{R}_i)+\text{c.c.}],\\
u_{i,z} &= \tfrac{1}{2}C'\,[\exp(i\mathbf{k}'_z\cdot\mathbf{R}_i)+\text{c.c.}]\,.
\end{aligned}
\tag{3}
$$

Here, $A$, $B$, and $C$ (respectively, $A'$, $B'$, and $C'$) are scalars quantifying the magnitude of the Cartesian components of $\boldsymbol{\omega}_i$ (respectively, $\mathbf{u}_i$); $\mathbf{R}_i$ is the lattice vector associated with cell $i$ and c.c. stands for "complex conjugate." Additionally, $\mathbf{k}_x$, $\mathbf{k}_y$, and $\mathbf{k}_z$ are $k$ vectors defining, respectively, the modulation of the $x$, $y$, and $z$ components of a general AFD distortion; for instance, we have $\mathbf{k}_x=\mathbf{k}_y=\frac{\pi}{a_{\text{lat}}}(\mathbf{x}+\mathbf{y}+\mathbf{z})$ and $\mathbf{k}_z=\frac{\pi}{a_{\text{lat}}}(\mathbf{x}+\mathbf{y})$ in a material displaying a $a^-b^-c^+$ tilting pattern. Similarly, $\mathbf{k}'_x$, $\mathbf{k}'_y$, and $\mathbf{k}'_z$ characterize the long-range polar or antipolar distortions associated with the $u_{i,\alpha}$ vector components. For example, a pure tetragonal $P4mm$ state for which the polarization is lying along $z$ has $\mathbf{k}'_z=\mathbf{0}$, while the AFE displacements inherent to the prototypical orthorhombic $a^-a^-c^+$ phase are associated with $\mathbf{k}'_x=\mathbf{k}'_y=\frac{\pi}{a_{\text{lat}}}\mathbf{z}$ (see, e.g., Ref. 19).

It is straightforward to show that inserting Eq. (3) into Eqs. (1) and (2) gives

$$\begin{aligned}\Delta E_1/(K_1 N) = {} & a_1 \sum_{\mathbf{G}} \delta(\mathbf{G}-\mathbf{k}'_z-\mathbf{k}_y-\mathbf{k}_z) + a_2 \sum_{\mathbf{G}} \delta(\mathbf{G}-\mathbf{k}'_z-\mathbf{k}_x-\mathbf{k}_z) + a_3 \sum_{\mathbf{G}} \delta(\mathbf{G}-\mathbf{k}'_x-\mathbf{k}_z-\mathbf{k}_x) \\ & + a_4 \sum_{\mathbf{G}} \delta(\mathbf{G}-\mathbf{k}'_x-\mathbf{k}_y-\mathbf{k}_x) + a_5 \sum_{\mathbf{G}} \delta(\mathbf{G}-\mathbf{k}'_y-\mathbf{k}_x-\mathbf{k}_y) + a_6 \sum_{\mathbf{G}} \delta(\mathbf{G}-\mathbf{k}'_y-\mathbf{k}_z-\mathbf{k}_y) \\ & + [\mathbf{k}_x \to -\mathbf{k}_x] + \cdots + [\mathbf{k}_x \to -\mathbf{k}_x; \mathbf{k}'_x \to -\mathbf{k}'_x] + \cdots \end{aligned} \tag{4}$$

and

$$\begin{aligned}\Delta E_2/(K_2 N) = {} & b_1 \sum_{\mathbf{G}} \delta(\mathbf{G}-\mathbf{k}'_z-2\mathbf{k}_y-\mathbf{k}_z) + b_2 \sum_{\mathbf{G}} \delta(\mathbf{G}-\mathbf{k}'_z-2\mathbf{k}_x-\mathbf{k}_z) + b_3 \sum_{\mathbf{G}} \delta(\mathbf{G}-\mathbf{k}'_x-2\mathbf{k}_z-\mathbf{k}_x) \\ & + b_4 \sum_{\mathbf{G}} \delta(\mathbf{G}-\mathbf{k}'_x-2\mathbf{k}_y-\mathbf{k}_x) + b_5 \sum_{\mathbf{G}} \delta(\mathbf{G}-\mathbf{k}'_y-2\mathbf{k}_x-\mathbf{k}_y) + b_6 \sum_{\mathbf{G}} \delta(\mathbf{G}-\mathbf{k}'_y-2\mathbf{k}_z-\mathbf{k}_y) \\ & + [\mathbf{k}_x \to -\mathbf{k}_x] + \cdots + [\mathbf{k}_x \to -\mathbf{k}_x; \mathbf{k}'_x \to -\mathbf{k}'_x] + \cdots , \end{aligned} \tag{5}$$

where $N$ is the number of cells in the crystal and $\mathbf{G}$ labels the reciprocal lattice vectors corresponding to the five-atom cubic perovskite structure. The terms that we have written explicitly are obtained from products of the first summands in Eq. (3) [e.g., the summand proportional to $\exp(i\mathbf{k}_x \cdot \mathbf{R}_i)$ in the case of $\omega_{i,x}$, etc.] plus the corresponding complex conjugates. Additional terms are indicated symbolically in Eqs. (4) and (5); thus, for example, $[\mathbf{k}_x \to -\mathbf{k}_x]$ denotes all the terms that can be derived from those explicitly written and involving $\omega_{i,x}$ by making the $\mathbf{k}_x \to -\mathbf{k}_x$ substitution. The $a$ and $b$ coefficients depend on the wave vectors as well, and are given by

$$\begin{aligned} a_1 = {} & \tfrac{1}{8} BCC'\{1 + \exp[i(\mathbf{k}_y+\mathbf{k}_z)\cdot a_{\text{lat}}\mathbf{x}] + \exp[i(\mathbf{k}_y+\mathbf{k}_z)\cdot a_{\text{lat}}\mathbf{z}] + \exp[i(\mathbf{k}_y+\mathbf{k}_z)\cdot a_{\text{lat}}(\mathbf{x}+\mathbf{z})] - \exp[i(\mathbf{k}_y+\mathbf{k}_z)\cdot a_{\text{lat}}(\mathbf{x}+\mathbf{y})] \\ & - \exp[i(\mathbf{k}_y+\mathbf{k}_z)\cdot a_{\text{lat}}\mathbf{y}] - \exp[i(\mathbf{k}_y+\mathbf{k}_z)\cdot a_{\text{lat}}(\mathbf{y}+\mathbf{z})] - \exp[i(\mathbf{k}_y+\mathbf{k}_z)\cdot a_{\text{lat}}(\mathbf{x}+\mathbf{y}+\mathbf{z})]\} + \text{ c.c.}, \end{aligned} \tag{6}$$

$$\begin{aligned} a_2 = {} & \tfrac{1}{8} ACC'\{1 + \exp[i(\mathbf{k}_x+\mathbf{k}_z)\cdot a_{\text{lat}}\mathbf{y}] + \exp[i(\mathbf{k}_x+\mathbf{k}_z)\cdot a_{\text{lat}}\mathbf{z}] + \exp[i(\mathbf{k}_x+\mathbf{k}_z)\cdot a_{\text{lat}}(\mathbf{y}+\mathbf{z})] - \exp[i(\mathbf{k}_x+\mathbf{k}_z)\cdot a_{\text{lat}}(\mathbf{x}+\mathbf{y})] \\ & - \exp[i(\mathbf{k}_x+\mathbf{k}_z)\cdot a_{\text{lat}}\mathbf{x}] - \exp[i(\mathbf{k}_x+\mathbf{k}_z)\cdot a_{\text{lat}}(\mathbf{x}+\mathbf{z})] - \exp[i(\mathbf{k}_x+\mathbf{k}_z)\cdot a_{\text{lat}}(\mathbf{x}+\mathbf{y}+\mathbf{z})]\} + \text{c.c.}, \end{aligned} \tag{7}$$

$$\begin{aligned} a_3 = {} & \tfrac{1}{8} ACA'\{1 + \exp[i(\mathbf{k}_x+\mathbf{k}_z)\cdot a_{\text{lat}}\mathbf{y}] + \exp[i(\mathbf{k}_x+\mathbf{k}_z)\cdot a_{\text{lat}}\mathbf{x}] + \exp[i(\mathbf{k}_x+\mathbf{k}_z)\cdot a_{\text{lat}}(\mathbf{x}+\mathbf{y})] - \exp[i(\mathbf{k}_x+\mathbf{k}_z)\cdot a_{\text{lat}}(\mathbf{y}+\mathbf{z})] \\ & - \exp[i(\mathbf{k}_x+\mathbf{k}_z)\cdot a_{\text{lat}}\mathbf{z}] - \exp[i(\mathbf{k}_x+\mathbf{k}_z)\cdot a_{\text{lat}}(\mathbf{x}+\mathbf{z})] - \exp[i(\mathbf{k}_x+\mathbf{k}_z)\cdot a_{\text{lat}}(\mathbf{x}+\mathbf{y}+\mathbf{z})]\} + \text{c.c.}, \end{aligned} \tag{8}$$

$$\begin{aligned} a_4 = {} & \tfrac{1}{8} ABA'\{1 + \exp[i(\mathbf{k}_x+\mathbf{k}_y)\cdot a_{\text{lat}}\mathbf{z}] + \exp[i(\mathbf{k}_x+\mathbf{k}_y)\cdot a_{\text{lat}}\mathbf{x}] + \exp[i(\mathbf{k}_x+\mathbf{k}_y)\cdot a_{\text{lat}}(\mathbf{x}+\mathbf{z})] - \exp[i(\mathbf{k}_x+\mathbf{k}_y)\cdot a_{\text{lat}}(\mathbf{y}+\mathbf{z})] \\ & - \exp[i(\mathbf{k}_x+\mathbf{k}_y)\cdot a_{\text{lat}}\mathbf{y}] - \exp[i(\mathbf{k}_x+\mathbf{k}_y)\cdot a_{\text{lat}}(\mathbf{y}+\mathbf{z})] - \exp[i(\mathbf{k}_x+\mathbf{k}_y)\cdot a_{\text{lat}}(\mathbf{x}+\mathbf{y}+\mathbf{z})]\} + \text{c.c.}, \end{aligned} \tag{9}$$

$$\begin{aligned} a_5 = {} & \tfrac{1}{8} ABB'\{1 + \exp[i(\mathbf{k}_x+\mathbf{k}_y)\cdot a_{\text{lat}}\mathbf{z}] + \exp[i(\mathbf{k}_x+\mathbf{k}_y)\cdot a_{\text{lat}}\mathbf{y}] + \exp[i(\mathbf{k}_x+\mathbf{k}_y)\cdot a_{\text{lat}}(\mathbf{y}+\mathbf{z})] - \exp[i(\mathbf{k}_x+\mathbf{k}_y)\cdot a_{\text{lat}}(\mathbf{x}+\mathbf{z})] \\ & - \exp[i(\mathbf{k}_x+\mathbf{k}_y)\cdot a_{\text{lat}}\mathbf{x}] - \exp[i(\mathbf{k}_x+\mathbf{k}_y)\cdot a_{\text{lat}}(\mathbf{x}+\mathbf{y})] - \exp[i(\mathbf{k}_x+\mathbf{k}_y)\cdot a_{\text{lat}}(\mathbf{x}+\mathbf{y}+\mathbf{z})]\} + \text{c.c.}, \end{aligned} \tag{10}$$

$$\begin{aligned} a_6 = {} & \tfrac{1}{8} BCB'\{1 + \exp[i(\mathbf{k}_y+\mathbf{k}_z)\cdot a_{\text{lat}}\mathbf{x}] + \exp[i(\mathbf{k}_y+\mathbf{k}_z)\cdot a_{\text{lat}}\mathbf{y}] + \exp[i(\mathbf{k}_y+\mathbf{k}_z)\cdot a_{\text{lat}}(\mathbf{x}+\mathbf{y})] - \exp[i(\mathbf{k}_y+\mathbf{k}_z)\cdot a_{\text{lat}}(\mathbf{x}+\mathbf{z})] \\ & - \exp[i(\mathbf{k}_y+\mathbf{k}_z)\cdot a_{\text{lat}}\mathbf{z}] - \exp[i(\mathbf{k}_y+\mathbf{k}_z)\cdot a_{\text{lat}}(\mathbf{y}+\mathbf{z})] - \exp[i(\mathbf{k}_y+\mathbf{k}_z)\cdot a_{\text{lat}}(\mathbf{x}+\mathbf{y}+\mathbf{z})]\} + \text{c.c.}, \end{aligned} \tag{11}$$

$$\begin{aligned} b_1 = {} & \tfrac{1}{16} B^2CC'\{\exp[i(2\mathbf{k}_y+\mathbf{k}_z)\cdot a_{\text{lat}}\mathbf{x}] + \exp[i(2\mathbf{k}_y+\mathbf{k}_z)\cdot a_{\text{lat}}\mathbf{z}] + \exp[i(2\mathbf{k}_y+\mathbf{k}_z)\cdot a_{\text{lat}}\mathbf{y}] + \exp[i(2\mathbf{k}_y+\mathbf{k}_z)\cdot a_{\text{lat}}(\mathbf{x}+\mathbf{y}+\mathbf{z})] \\ & - 1 - \exp[i(2\mathbf{k}_y+\mathbf{k}_z)\cdot a_{\text{lat}}(\mathbf{x}+\mathbf{z})] + \exp[i(2\mathbf{k}_y+\mathbf{k}_z)\cdot a_{\text{lat}}(\mathbf{x}+\mathbf{y})] + \exp[i(2\mathbf{k}_y+\mathbf{k}_z)\cdot a_{\text{lat}}(\mathbf{y}+\mathbf{z})]\} + \text{c.c.}, \end{aligned} \tag{12}$$

$$\begin{aligned} b_2 = {} & \tfrac{1}{16} A^2CC'\{1 + \exp[i(2\mathbf{k}_x+\mathbf{k}_z)\cdot a_{\text{lat}}(\mathbf{y}+\mathbf{z})] + \exp[i(2\mathbf{k}_x+\mathbf{k}_z)\cdot a_{\text{lat}}(\mathbf{x}+\mathbf{y})] + \exp[i(2\mathbf{k}_x+\mathbf{k}_z)\cdot a_{\text{lat}}(\mathbf{x}+\mathbf{z})] \\ & - \exp[i(2\mathbf{k}_x+\mathbf{k}_z)\cdot a_{\text{lat}}\mathbf{y}] - \exp[i(2\mathbf{k}_x+\mathbf{k}_z)\cdot a_{\text{lat}}\mathbf{z}] - \exp[i(2\mathbf{k}_x+\mathbf{k}_z)\cdot a_{\text{lat}}\mathbf{x}] - \exp[i(2\mathbf{k}_x+\mathbf{k}_z)\cdot a_{\text{lat}}(\mathbf{x}+\mathbf{y}+\mathbf{z})]\} + \text{c.c.}, \end{aligned} \tag{13}$$

$$\begin{aligned} b_3 = {} & \tfrac{1}{16} AC^2A'\{\exp[i(\mathbf{k}_x+2\mathbf{k}_z)\cdot a_{\text{lat}}\mathbf{y}] + \exp[i(\mathbf{k}_x+2\mathbf{k}_z)\cdot a_{\text{lat}}\mathbf{x}] + \exp[i(\mathbf{k}_x+2\mathbf{k}_z)\cdot a_{\text{lat}}\mathbf{z}] + \exp[i(\mathbf{k}_x+2\mathbf{k}_z)\cdot a_{\text{lat}}(\mathbf{x}+\mathbf{y}+\mathbf{z})] \\ & - 1 - \exp[i(\mathbf{k}_x+2\mathbf{k}_z)\cdot a_{\text{lat}}(\mathbf{x}+\mathbf{y})] - \exp[i(\mathbf{k}_x+2\mathbf{k}_z)\cdot a_{\text{lat}}(\mathbf{y}+\mathbf{z})] - \exp[i(\mathbf{k}_x+2\mathbf{k}_z)\cdot a_{\text{lat}}(\mathbf{x}+\mathbf{z})]\} + \text{c.c.}, \end{aligned} \tag{14}$$

$$\begin{aligned} b_4 = {} & \tfrac{1}{16} AB^2A'\{1 + \exp[i(\mathbf{k}_x+2\mathbf{k}_y)\cdot a_{\text{lat}}(\mathbf{x}+\mathbf{z})] + \exp[i(\mathbf{k}_x+2\mathbf{k}_y)\cdot a_{\text{lat}}(\mathbf{y}+\mathbf{z})] + \exp[i(\mathbf{k}_x+2\mathbf{k}_y)\cdot a_{\text{lat}}(\mathbf{x}+\mathbf{y})] \\ & - \exp[i(\mathbf{k}_x+2\mathbf{k}_y)\cdot a_{\text{lat}}\mathbf{z}] - \exp[i(\mathbf{k}_x+2\mathbf{k}_y)\cdot a_{\text{lat}}\mathbf{x}] - \exp[i(\mathbf{k}_x+2\mathbf{k}_y)\cdot a_{\text{lat}}\mathbf{y}] - \exp[i(\mathbf{k}_x+2\mathbf{k}_y)\cdot a_{\text{lat}}(\mathbf{x}+\mathbf{y}+\mathbf{z})]\} + \text{c.c.}, \end{aligned} \tag{15}$$

$$\begin{aligned} b_5 = {} & \tfrac{1}{16} A^2BB'\{\exp[i(2\mathbf{k}_x+\mathbf{k}_y)\cdot a_{\text{lat}}\mathbf{z}] + \exp[i(2\mathbf{k}_x+\mathbf{k}_y)\cdot a_{\text{lat}}\mathbf{y}] + \exp[i(2\mathbf{k}_x+\mathbf{k}_y)\cdot a_{\text{lat}}\mathbf{x}] + \exp[i(2\mathbf{k}_x+\mathbf{k}_y)\cdot a_{\text{lat}}(\mathbf{x}+\mathbf{y}+\mathbf{z})] \\ & - 1 - \exp[i(2\mathbf{k}_x+\mathbf{k}_y)\cdot a_{\text{lat}}(\mathbf{y}+\mathbf{z})] - \exp[i(2\mathbf{k}_x+\mathbf{k}_y)\cdot a_{\text{lat}}(\mathbf{x}+\mathbf{z})] - \exp[i(2\mathbf{k}_x+\mathbf{k}_y)\cdot a_{\text{lat}}(\mathbf{x}+\mathbf{y})]\} + \text{c.c.}, \end{aligned} \tag{16}$$

and

$$\begin{aligned} b_6 = {} & \tfrac{1}{16} BC^2B'\{1 + \exp[i(\mathbf{k}_y+2\mathbf{k}_z)\cdot a_{\text{lat}}(\mathbf{x}+\mathbf{y})] + \exp[i(\mathbf{k}_y+2\mathbf{k}_z)\cdot a_{\text{lat}}(\mathbf{x}+\mathbf{z})] + \exp[i(\mathbf{k}_y+2\mathbf{k}_z)\cdot a_{\text{lat}}(\mathbf{y}+\mathbf{z})] \\ & - \exp[i(\mathbf{k}_y+2\mathbf{k}_z)\cdot a_{\text{lat}}\mathbf{x}] - \exp[i(\mathbf{k}_y+2\mathbf{k}_z)\cdot a_{\text{lat}}\mathbf{y}] - \exp[i(\mathbf{k}_y+2\mathbf{k}_z)\cdot a_{\text{lat}}\mathbf{z}] - \exp[i(\mathbf{k}_y+2\mathbf{k}_z)\cdot a_{\text{lat}}(\mathbf{x}+\mathbf{y}+\mathbf{z})]\} + \text{c.c.} \end{aligned} \tag{17}$$

TABLE I. $k$ vectors associated with AFE motions induced by simple AFD patterns. The AFE displacements are further characterized by the $a$ and $b$ parameters of Eqs. (6)–(17) and the direction along which the $A$ cations displace. All given $k$ vectors must be multiplied by the factor $\pi/a_{\text{lat}}$, which has been omitted for clarity.

| AFD pattern | AFD $k$ vectors | AFE $k$ vectors | AFE coefficients | AFE displacements |
|---|---|---|---|---|
| $a^0a^0c^-$ | $\mathbf{k}_z = \mathbf{x}+\mathbf{y}+\mathbf{z}$ | None | N/A | N/A |
| $a^0a^0c^+$ | $\mathbf{k}_z = \mathbf{x}+\mathbf{y}$ | None | N/A | N/A |
| $a^+b^+c^0$ | $\mathbf{k}_x = \mathbf{y}+\mathbf{z}$<br>$\mathbf{k}_y = \mathbf{x}+\mathbf{z}$ | None | N/A | N/A |
| $a^-b^-c^0$ | $\mathbf{k}_x = \mathbf{x}+\mathbf{y}+\mathbf{z}$<br>$\mathbf{k}_y = \mathbf{x}+\mathbf{y}+\mathbf{z}$ | $\mathbf{k}'_x = \mathbf{x}+\mathbf{y}+\mathbf{z}$<br>$\mathbf{k}'_y = \mathbf{x}+\mathbf{y}+\mathbf{z}$ | $b_4 = AB^2A'$<br>$b_5 = -A^2BB'$ | $[v\bar{v}'0]$ |
| $a^-a^-c^0$ | $\mathbf{k}_x = \mathbf{x}+\mathbf{y}+\mathbf{z}$<br>$\mathbf{k}_y = \mathbf{x}+\mathbf{y}+\mathbf{z}$ | $\mathbf{k}'_x = \mathbf{x}+\mathbf{y}+\mathbf{z}$<br>$\mathbf{k}'_y = \mathbf{x}+\mathbf{y}+\mathbf{z}$ | $b_4 = A^3A'$<br>$b_5 = -A^3A'$ | $[1\bar{1}0]$ |
| $a^-b^+c^0$ | $\mathbf{k}_x = \mathbf{x}+\mathbf{y}+\mathbf{z}$<br>$\mathbf{k}_y = \mathbf{x}+\mathbf{z}$ | $\mathbf{k}'_x = \mathbf{y}$<br>$\mathbf{k}'_x = \mathbf{x}+\mathbf{y}+\mathbf{z}$ | $a_4 = 2ABA'$<br>$a_4 = 2ABA'$ | [100] |
| $a^+b^+c^+$ | $\mathbf{k}_x = \mathbf{y}+\mathbf{z}$<br>$\mathbf{k}_y = \mathbf{x}+\mathbf{z}$<br>$\mathbf{k}_z = \mathbf{x}+\mathbf{y}$ | None | N/A | N/A |
| $a^-b^-c^-$ | $\mathbf{k}_x = \mathbf{x}+\mathbf{y}+\mathbf{z}$<br>$\mathbf{k}_y = \mathbf{x}+\mathbf{y}+\mathbf{z}$<br>$\mathbf{k}_z = \mathbf{x}+\mathbf{y}+\mathbf{z}$ | $\mathbf{k}'_x = \mathbf{x}+\mathbf{y}+\mathbf{z}$<br>$\mathbf{k}'_y = \mathbf{x}+\mathbf{y}+\mathbf{z}$<br>$\mathbf{k}'_z = \mathbf{x}+\mathbf{y}+\mathbf{z}$ | $b_4+b_3 = AA'(B^2-C^2)$<br>$b_6+b_5 = BB'(C^2-A^2)$<br>$b_2+b_1 = CC'(A^2-B^2)$ | $[vv'v'']$ |
| $a^-a^-a^-$ | $\mathbf{k}_x = \mathbf{x}+\mathbf{y}+\mathbf{z}$<br>$\mathbf{k}_y = \mathbf{x}+\mathbf{y}+\mathbf{z}$<br>$\mathbf{k}_z = \mathbf{x}+\mathbf{y}+\mathbf{z}$ | None | N/A | N/A |
| $a^-a^-c^-$ | $\mathbf{k}_x = \mathbf{x}+\mathbf{y}+\mathbf{z}$<br>$\mathbf{k}_y = \mathbf{x}+\mathbf{y}+\mathbf{z}$<br>$\mathbf{k}_z = \mathbf{x}+\mathbf{y}+\mathbf{z}$ | $\mathbf{k}'_x = \mathbf{x}+\mathbf{y}+\mathbf{z}$<br>$\mathbf{k}'_y = \mathbf{x}+\mathbf{y}+\mathbf{z}$ | $b_4+b_3 = AA'(B^2-C^2)$<br>$b_6+b_5 = -AA'(B^2-C^2)$ | $[1\bar{1}0]$ |
| $a^-b^-c^+$ | $\mathbf{k}_x = \mathbf{x}+\mathbf{y}+\mathbf{z}$<br>$\mathbf{k}_y = \mathbf{x}+\mathbf{y}+\mathbf{z}$<br>$\mathbf{k}_z = \mathbf{x}+\mathbf{y}$ | $\mathbf{k}'_x = \mathbf{z}$<br>$\mathbf{k}'_y = \mathbf{z}$<br>$\mathbf{k}'_x = \mathbf{x}+\mathbf{y}+\mathbf{z}$<br>$\mathbf{k}'_y = \mathbf{x}+\mathbf{y}+\mathbf{z}$ | $a_3 = 2ACA'$<br>$a_6 = 2BCB'$<br>$b_4+b_3 = AA'(B^2-C^2)$<br>$b_6+b_5 = BB'(C^2-A^2)$ | $[vv'0]$<br>and<br>$[v''v'''0]$ |
| $a^-a^-c^+$ | $\mathbf{k}_x = \mathbf{x}+\mathbf{y}+\mathbf{z}$<br>$\mathbf{k}_y = \mathbf{x}+\mathbf{y}+\mathbf{z}$<br>$\mathbf{k}_z = \mathbf{x}+\mathbf{y}$ | $\mathbf{k}'_x = \mathbf{z}$<br>$\mathbf{k}'_y = \mathbf{z}$<br>$\mathbf{k}'_x = \mathbf{x}+\mathbf{y}+\mathbf{z}$<br>$\mathbf{k}'_y = \mathbf{x}+\mathbf{y}+\mathbf{z}$ | $a_3 = 2ACA'$<br>$a_6 = 2ACA'$<br>$b_4+b_3 = AA'(B^2-C^2)$<br>$b_6+b_5 = -AA'(B^2-C^2)$ | [110]<br>and<br>$[1\bar{1}0]$ |
| $a^+b^+c^-$ | $\mathbf{k}_x = \mathbf{y}+\mathbf{z}$<br>$\mathbf{k}_y = \mathbf{x}+\mathbf{z}$<br>$\mathbf{k}_z = \mathbf{x}+\mathbf{y}+\mathbf{z}$ | $\mathbf{k}'_z = \mathbf{y}$<br>$\mathbf{k}'_z = \mathbf{x}$<br>$\mathbf{k}'_z = \mathbf{x}+\mathbf{y}+\mathbf{z}$ | $a_1 = 2BCC'$<br>$a_2 = 2ACC'$<br>$b_2+b_1 = CC'(A^2-B^2)$ | [001] |
| $a^+a^+c^-$ | $\mathbf{k}_x = \mathbf{y}+\mathbf{z}$<br>$\mathbf{k}_y = \mathbf{x}+\mathbf{z}$<br>$\mathbf{k}_z = \mathbf{x}+\mathbf{y}+\mathbf{z}$ | $\mathbf{k}'_z = \mathbf{y}$<br>$\mathbf{k}'_z = \mathbf{x}$ | $a_1 = 2BCC'$<br>$a_2 = 2BCC'$ | [001] |

## III. EXAMPLES OF APPLICATION

### A. Simple tilting patterns

Let us now apply the above equations to "simple" AFD patterns and thus check whether (and what kind of) AFE displacements are automatically induced. The results are summarized in Table I, while we further discuss and explain them in details below. Note that, for all the simple AFD patterns, the components of the corresponding $\mathbf{k}$ vectors are either 0 or $\pi/a_{\text{lat}}$. As a result, it can be seen that all the extra terms indicated in Eqs. (4) and (5), which are obtained by making substitutions of the type $\mathbf{k} \to -\mathbf{k}$, reduce to those explicitly written. Hence, in order to determine which AFE patterns are induced by simple AFD tilts, it is not necessary to consider such extra terms, and we do not discuss them in the following. Nevertheless, note that the contribution of the extra terms would need to be considered in a quantitative calculation of the AFD-induced AFE distortions.

#### *1. $a^0a^0c^-$ and $a^0a^0c^+$ patterns*

Our expressions for $\Delta E_1$ [see Eq. (1)] and $\Delta E_2$ [see Eq. (2)] indicate that *no* AFE motions appear as a consequence of the $a^0a^0c^-$ and $a^0a^0c^+$ patterns, since one needs to have rotations about *at least two* pseudocubic axes to induce nonzero $\mathbf{u}_i$ values.

#### 2. $a^+b^+c^0$, $a^-b^-c^0$, and $a^-b^+c^0$ patterns

Let us now consider the general case in which we have rotations about two pseudocubic axes. This possibility includes the $a^+b^+c^0$, $a^-b^-c^0$, and $a^-b^+c^0$ patterns. In all such cases, the coefficients $a_1$, $a_2$, $a_3$, $a_6$, $b_1$, $b_2$, $b_3$, and $b_6$ vanish; this is a result of having $C = 0$ [see Eq. (3)], i.e., no rotation about the third pseudocubic axis.

Then, for the $a^+b^+c^0$ pattern, we have $\mathbf{k}_x = \frac{\pi}{a_{\text{lat}}}(\mathbf{y}+\mathbf{z})$ and $\mathbf{k}_y = \frac{\pi}{a_{\text{lat}}}(\mathbf{x}+\mathbf{z})$, which renders $a_4$, $a_5$, $b_4$ and $b_5$ null according to the equations above. In other words, there are no AFE motions associated with the $a^+b^+c^0$ pattern.

On the other hand, for $a^-b^-c^0$, we have $\mathbf{k}_x = \mathbf{k}_y = \frac{\pi}{a_{\text{lat}}}(\mathbf{x}+\mathbf{y}+\mathbf{z})$, which makes $a_4$ and $a_5$ vanish, but leads to $b_4$ and $b_5$ equal to $AB^2A'$ and $-A^2BB'$, respectively. Moreover, we obtain such a nonzero result for $\mathbf{k}'_x = \mathbf{k}'_y = \frac{\pi}{a_{\text{lat}}}(\mathbf{x}+\mathbf{y}+\mathbf{z})$. In other words, we predict that the $a^-b^-c^0$ pattern will induce AFE displacements along the $\pm[v\bar{v}'0]$ pseudocubic direction, and these displacements will be modulated in antiphase when going from one $A$ site to any of its six nearest-neighboring $A$ sites. Interestingly, $v$ can be different from $v'$ in the general case. Yet, according to Eq. (3) the $[v\bar{v}'0]$ direction becomes exactly $[1\bar{1}0]$ when $A' = B'$ and $A = B$, that is, when $b_4 = b_5$. This only occurs when the oxygen octahedral tilting about [100] is equal in magnitude to that about [010], i.e., when $a^-b^-c^0$ is, in fact, the $a^-a^-c^0$ pattern. This kind of AFE displacements is exactly the one found by first-principles calculations for the $Ima2$ phase of $BiFeO_3$,[18] which adopts the $a^-a^-c^0$ rotational order.

Similarly, in the case of $a^-b^+c^0$, one can see that the only nonzero coefficients are $a_4 = 2ABA'$ and $b_4 = AB^2A'$; the associated Dirac functions in Eqs. (4) and (5) yield two solutions for $\mathbf{k}'_x$, namely, $\mathbf{k}'_x = \frac{\pi}{a_{\text{lat}}}\mathbf{y}$ and $\mathbf{k}'_x = \frac{\pi}{a_{\text{lat}}}(\mathbf{x}+\mathbf{y}+\mathbf{z})$. As a result, the $a^-b^+c^0$ pattern will induce AFE motions with the $A$ atoms moving along the pseudocubic $\pm[100]$ direction and having two differently modulated components, i.e., one that changes sign when moving between (010) AO planes and a second one changing sign when going from one $A$ site to any of its six first nearest neighbors in the $A$ sublattice.

#### 3. $a^+b^+c^+$, $a^-b^-c^-$, $a^-b^-c^+$, and $a^+b^+c^-$ patterns

Let us now concentrate on the patterns that involve rotations about all three pseudocubic axes, which include $a^+b^+c^+$, $a^-b^-c^-$, $a^-b^-c^+$, and $a^+b^+c^-$. These cases can, in fact, be resolved by realizing that the terms in Eqs. (1) and (2) involve *only two* components of the $\omega$ vectors; hence, we can treat the cases involving three different components as the addition of pairs.

For instance, we can think of $a^+b^+c^+$ as being a combination of $a^+b^+c^0$, $a^0b^+c^+$, and $a^+b^0c^+$. It is then trivial to understand why there is no tilting-driven AFE motions in any $a^+b^+c^+$ system, since the $a^+b^+c^0$ pattern has been previously found to present no AFE displacements (see Table I) and we note that the $a^0b^+c^+$ and $a^+b^0c^+$ cases can be deduced from the $a^+b^+c^0$ result by circular permutation.

Similarly, by treating the $a^-b^-c^-$ pattern as being the addition of $a^-b^-c^0$, $a^0b^-c^-$, and $a^-b^0c^-$, and recalling the result for $a^-b^-c^0$ summarized in Table I (from which the other cases can be derived by appropriate permutations), we obtain AFE distortions associated to $\mathbf{k}'_x = \mathbf{k}'_y = \mathbf{k}'_z = \frac{\pi}{a_{\text{lat}}}(\mathbf{x}+\mathbf{y}+\mathbf{z})$, with the corresponding parameters being $b_4 + b_3 = A(B^2 - C^2)A'$, $b_6 + b_5 = B(C^2 - A^2)B'$, and $b_2 + b_1 = C(A^2 - B^2)C'$, respectively. In other words, the $a^-b^-c^-$ pattern induces AFE displacements along $\pm[vv'v'']$, and such displacements are modulated in antiphase along the three pseudocubic directions. Interestingly, for the particular case of $a^-a^-a^-$ (i.e., when *all* the antiphase tiltings have the same magnitude), we have $A = B = C$ and, as a result, the coefficients $b_4 + b_3$, $b_6 + b_5$, and $b_2 + b_1$ are all annihilated; hence the $a^-a^-a^-$ pattern has no AFE displacements associated to it. This is, for example, the case of the rhombohedral $R3c$ phase of $BiFeO_3$, which is stable at ambient conditions. On the other hand, the $a^-a^-c^-$ pattern should exhibit AFE displacements along the $\pm[1\bar{1}0]$ direction. Indeed, in that case $A = B \neq C$ and, therefore, $b_4 + b_3 = A(B^2 - C^2)A'$ and $b_6 + b_5 = B(C^2 - A^2)B'$ do not vanish; further, it can be seen that in this case the energy minimum satisfies $A' = B'$, which renders $b_4 + b_3 = -b_6 - b_5$. This kind of AFE displacements has indeed been reported in the $Cc$ phase of $BiFeO_3$, which displays a $a^-a^-c^-$ pattern.[18]

Similar arguments can be used to prove that, for the $a^-b^-c^+$ pattern: (i) the $\Delta E_1$ term leads to $\mathbf{k}'_x = \frac{\pi}{a_{\text{lat}}}\mathbf{z}$ and $\mathbf{k}'_y = \frac{\pi}{a_{\text{lat}}}\mathbf{z}$, with the corresponding nonzero parameters being $a_3 = 2ACA'$ and $a_6 = 2BCB'$, respectively, and (ii) $\Delta E_2$ results in $\mathbf{k}'_x = \frac{\pi}{a_{\text{lat}}}(\mathbf{x}+\mathbf{y}+\mathbf{z})$ and $\mathbf{k}'_y = \frac{\pi}{a_{\text{lat}}}(\mathbf{x}+\mathbf{y}+\mathbf{z})$ with the associated coefficients being $b_4 + b_3 = A(B^2 - C^2)A'$ and $b_6 + b_5 = B(C^2 - A^2)B'$. The $a^-b^-c^+$ pattern therefore adopts AFE displacements of two types: one type is along the $\pm[vv'0]$ direction and has an antiphase modulation when going from one (001) AO plane to an adjacent (001) AO plane, while the second one involves $A$-atom displacements along the $\pm[v''v'''0]$ direction and is modulated in antiphase along the three pseudocubic directions of the perovskite lattice. (Here, $v$, $v'$, $v''$, and $v'''$ can all be different from each other.) Moreover, for the $a^-a^-c^+$ pattern, we have $A = B$, and one can easily prove that the $[vv'0]$ and $[v''v'''0]$ directions become [110] and $[1\bar{1}0]$, respectively. This is precisely what is known to occur in the orthorhombic $Pnma$ phase that is ubiquitous among perovskite oxides (see, e.g., Ref. 19).

Regarding the $a^+b^+c^-$ pattern, splitting it into $a^+b^+c^0$, $a^0b^+c^-$, and $a^+b^0c^-$ results in (i) $\mathbf{k}'_z = \frac{\pi}{a_{\text{lat}}}\mathbf{y}$ and $\mathbf{k}'_z = \frac{\pi}{a_{\text{lat}}}\mathbf{x}$, with $a_1 = 2BCC'$ and $a_2 = 2ACC'$, respectively, for the AFE motions arising from $\Delta E_1$ and (ii) $\mathbf{k}'_z = \frac{\pi}{a_{\text{lat}}}(\mathbf{x}+\mathbf{y}+\mathbf{z})$, associated with $b_2 + b_1 = C(A^2 - B^2)C'$, for the AFE distortions coming from $\Delta E_2$. The AFE motions therefore lie along the $\pm[001]$ pseudocubic direction and include *three* different contributions: the first one changes sign as we move from one (010) AO plane to the next one, the second AFE pattern reverses its direction every other (100) AO plane, and the third one is modulated in antiphase along all three pseudocubic directions. Interestingly, in the $a^+a^+c^-$ pattern ($A = B \neq C$), the third distortion vanishes and the first and second ones have the same magnitude. Consequently, one can easily prove that only half of the $A$ cations move, along either [001] or $[00\bar{1}]$, in the $a^+a^+c^-$ case.

We tested the correctness of all the aforementioned predictions in the following way. (For this analysis, we made use of the web-based open-access tool ISODISTORT.[24]) In each

case, we considered the symmetry reduction resulting from the condensation of the specific AFD pattern in the ideal cubic perovskite phase; then, we derived the list of all the atomic displacements that are allowed in such a low-symmetry phase, and identified those involving the $A$ cations. It was found that *all* the predictions summarized in Table I are indeed correct, and that the AFE displacements arising from the $\Delta E_1$ and $\Delta E_2$ energies of Eqs. (1) and (2) correspond, in fact, to the AFE modes labeled $X_5^+$ and $R_5^+$, respectively. Thus, remarkably, our simple model energy predicts all the AFE displacements that can be induced by the occurrence of simple AFD patterns in perovskites, providing us with a intuitive and practical scheme for the analysis and straightforward prediction of such distortions. Further, Eqs. (1) and (2) also provide an atomistic picture of the physical couplings that actually induce the displacements.

### B. Complex tilting patterns

Let us now use our formalism to check whether AFE displacements can also occur in association with *complex* tilting patterns. For that, let us focus on the $\Delta E_1$ term [see Eq. (1)] and begin by considering the case of a rotational pattern denoted by $a^-b^-c^k$, where $c^k$ stands for a *complex* long-range AFD tilting about the [001] axis that is associated with neither the $M$ point $[\frac{\pi}{a_{\rm lat}}(\mathbf{x}+\mathbf{y})]$ nor the $R$ point $[\frac{\pi}{a_{\rm lat}}(\mathbf{x}+\mathbf{y}+\mathbf{z})]$ of the first Brillouin zone corresponding to the five-atom cubic cell; rather, this complex pattern will be associated to a $k$ point in between. Hence we have $\mathbf{k}_x = \mathbf{k}_y = \frac{\pi}{a_{\rm lat}}(\mathbf{x}+\mathbf{y}+\mathbf{z})$, while $\mathbf{k}_z = \alpha\frac{\pi}{a_{\rm lat}}(\mathbf{x}+\mathbf{y}+\mathbf{z}) + \beta\frac{\pi}{a_{\rm lat}}(\mathbf{x}+\mathbf{y})$ with $\alpha+\beta=1$. Note that the resulting overall periodicity along the $z$ axis is $2/\alpha$ in terms of the number of five-atom unit cells. Figure 4 shows an example for $\alpha = 1/2$, with the $\omega_{i,z}$ rotation amplitudes modulated as "$++--$" as we move along the $z$ direction.

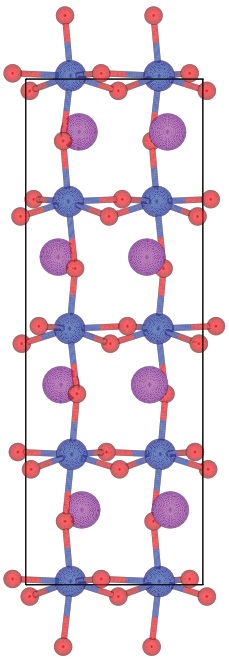

FIG. 4. (Color online) Sketch of complex AFD pattern $a^-a^-c^k$ with $\mathbf{k}_z = \frac{\pi}{a_{\rm lat}}(0,0,1/2)$. The peculiar pattern of $O_6$ rotations about the vertical axes gives rise to unusual AFE displacements of the $A$ cations in the $xy$ plane.

It is straightforward to prove that, for such a complex rotational pattern, and restricting ourselves to the terms explicitly written in Eq. (4), we have zero values for $a_1$, $a_2$, $a_4$, and $a_5$; additionally, we get $a_3 = ACA'[1+\cos(\alpha\pi)]$ and $a_6 = BCB'[1+\cos(\alpha\pi)]$. Moreover, from the $a_3$ and $a_6$ terms in Eq. (4), we get AFE displacements associated with $\mathbf{k}'_x = \mathbf{k}'_y = (1-\alpha)\frac{\pi}{a_{\rm lat}}\mathbf{z}$. In other words, our energy term $\Delta E_1$ implies that an $a^-b^-c^k$ pattern will induce exotic AFE displacements with the $A$ atoms moving along the $\pm[vv'0]$ pseudocubic direction and a modulation given by a $k$ vector between $\Gamma$ and $\frac{\pi}{a_{\rm lat}}\mathbf{z}$. This is exactly what is known to happen for the so-called nanoscale-twinned phases recently discovered in various perovskite systems, such as (Ca,Sr)$TiO_3$,[20] $BiFeO_3$,[21] and $EuTiO_3$.[22] As readily appreciated in Fig. 4, in that case the AFE distortion of the $A$ cations is associated to the $\frac{\pi}{2a_{\rm lat}}\mathbf{z}$ wave vector.

Our proposed energies also lead to the prediction of other AFE configurations, driven by AFD patterns, that have not been yet reported in the literature. For example, consider the case of $a^-b^+c^k$ for which each axis possesses different kinds of oxygen octahedra tilting, i.e., antiphase, in-phase, and complex, respectively. More precisely, we have $\mathbf{k}_x = \frac{\pi}{a_{\rm lat}}(\mathbf{x}+\mathbf{y}+\mathbf{z})$, $\mathbf{k}_y = \frac{\pi}{a_{\rm lat}}(\mathbf{x}+\mathbf{z})$, and $\mathbf{k}_z = \alpha\frac{\pi}{a_{\rm lat}}(\mathbf{x}+\mathbf{y}+\mathbf{z}) + \beta\frac{\pi}{a_{\rm lat}}(\mathbf{x}+\mathbf{y})$ with $\alpha+\beta=1$. It is easy to demonstrate that, for this particular case, the $\Delta E_1$ term leads to $\mathbf{k}'_z = \frac{\pi}{a_{\rm lat}}\mathbf{y} + (1-\alpha)\frac{\pi}{a_{\rm lat}}\mathbf{z}$, $\mathbf{k}'_x = \frac{\pi}{a_{\rm lat}}\mathbf{y}$, and $\mathbf{k}'_x = (1-\alpha)\frac{\pi}{a_{\rm lat}}\mathbf{z}$, with the corresponding coefficients $a_1 = BCC'[1-\cos(\alpha\pi)]$, $a_4 = 2ABB'$, and $a_3 = ACA'[1+\cos(\alpha\pi)]$. [Here again, we have restricted our analysis to the terms explicitly given in Eq. (4).] The $a^-b^+c^k$ pattern can therefore exhibit unusual AFE displacements with the $A$ cations moving even along the direction of the complex octahedral rotations, in contrast with the previous $a^-b^-c^k$ case. In addition, this AFD pattern would induce AFE motions along the $\pm[100]$ direction and modulated according to two different $k$ vectors, namely, one that involves a period of two lattice constants along $y$, and a second contribution involving a longer period along $z$. We hope that this prediction will be experimentally confirmed.

## IV. CONCLUSIONS

In summary, we have introduced two simple energy terms that couple, in a collaborative fashion and at an atomistic scale, the AFD motions and AFE distortions of the $A$-site cations of any $ABO_3$ perovskite. We have shown that these energy terms allow to reproduce and explain many $A$-site AFE patterns that have been seen to coexist with AFD distortions, may they be simple ones (i.e., expressible in Glazer's notation) or complex ones involving a large repeated unit. As a result of our analysis, we have also obtained novel combinations of AFD and AFE patterns that are awaiting to be experimentally seen.

The initial motivation and focus of this work was the investigation of situations in which the AFE distortions appear as a consequence of the symmetry breaking caused by the condensation of an AFD instability. Hence, in this sense, we are dealing with *improper antiferroelectrics*. On the other hand, we can imagine situations in which the $A$-site AFE distortion

constitutes an instability of the cubic perovskite structure by itself. (In fact, first-principles simulations show that this is the case in Bi-based perovskites like $BiFeO_3$.) In such *proper antiferroelectric* cases, the couplings here discussed would favor the occurrence of certain AFD patterns. In particular, $\Delta E_1$ could lead to a triggered-type phase transition involving specific $O_6$-octahedra rotations.[25–28]

It is also important to realize that our energy terms $\Delta E_1$ and $\Delta E_2$ can be incorporated in atomistic approaches, such as effective Hamiltonians,[21,23] in order to (i) investigate how the associated AFD and AFE patterns evolve with, e.g., temperature, applied electric fields, epitaxial strain, etc., and (ii) determine the results of the competition of the energies of Eqs. (1) and (2) with other (known) energies associated with polar, AFD, and strain degrees of freedom. For instance, it is worthwhile to realize that a previous effective Hamiltonian approach neglecting Eqs. (1) and (2) wrongly predicted a transition from $R3c$ to a simple tetragonal AFD phase in $BiFeO_3$ at around 1100 K and did not find the high-temperature $Pnma$ that this compound is known to present.[29] As shown in Ref. 21, such shortcomings were resolved when incorporating Eq. (1) into a revised effective Hamiltonian scheme.

Moreover, our coupling terms could also be used to capture the above-discussed effects in phenomenological Landau-like theories. A particularly relevant case is the investigation of orthorhombic $Pnma$ phases with the $a^-a^-c^+$ pattern, which constitute the ground state of many perovskite oxides.[30] Our work indicates that, in such a case, Eqs. (1) and (2) lead to (more compact) Landau potentials of the form $A_x\omega_{R,x}\omega_{M,z}$, $A_y\omega_{R,y}\omega_{M,z}$, $R_x\omega_{R,x}\omega_{M,z}^2$, and $R_y\omega_{R,y}\omega_{M,z}^2$; here, $A_x$ (respectively $A_y$) represents the long-range AFE order involving $A$-cation displacements along the $\pm$[100] (respectively $\pm$[010]) direction and displaying an $X$-like modulation given by the $\frac{\pi}{a_{\text{lat}}}\mathbf{z}$ $k$ point; $\omega_{R,x}$ (respectively $\omega_{R,y}$) is the long-range *antiphase* tilting pattern about the [100] (respectively [010]) axis and modulated in antiphase corresponding to the $R$-point of the first Brillouin zone; $\omega_{M,z}$ is the *in-phase* tilting about the $z$ axis associated with the zone-boundary $M$ point $\frac{\pi}{a_{\text{lat}}}(\mathbf{x}+\mathbf{y})$. Finally, $R_x$ (respectively $R_y$) are the AFE vectors describing motions of the $A$ atoms along the $\pm$[100] (respectively $\pm$[010]) direction and associated with the $R$ point of the first Brillouin zone.

Finally, let us note that, while our analysis corresponds to bulk $ABO_3$ compounds, it can be readily applied to the case of superlattices involving two or more types of cations. In particular, much attention is now being paid to $ABO_3$-$A'BO_3$ heterostructures, particularly after the discovery of unconventional forms of ferroelectricity in the $PbTiO_3$-$SrTiO_3$ system.[31] In such cases, because of the symmetry breaking imposed by the chemical modulation along the growth direction, the AFE-like modes involving the $A$ and $A'$ cations can actually have a *ferroelectric* character,[32] as the antiphase displacements of different cationic species do not need to perfectly compensate. Interestingly, since the local environment of the $A$ and $A'$ cations in an $ABO_3$-$A'BO_3$ superlattice is very similar to that of a simple $ABO_3$ structure, we can expect that the terms discussed in this paper will also dominate the AFD-induced $A$-cation displacements in that case. Hence our results can be easily applied to the discussion of AFD-induced AFE and FE distortions in superlattices.

The key role played by the AFD motions in determining the properties of perovskite materials, ranging from their conductivity to the emergence of novel polar orders, has been recently emphasized and is generating renewed interest in the community.[33] Our work is thus especially timely, as it explains important structural effects driven by the oxygen-octahedral rotations. We thus hope that our results will be of broad interest to both experimentalists and theorists working on perovskites.

## ACKNOWLEDGMENTS

We thank E. Salje for useful discussions. This work is mostly financially supported by NSF grant DMR-1066158. We also acknowledge ARO Grant W911NF-12-1-0085, ONR Grants N00014-11-1-0384 and N00014-08-1-0915, and Department of Energy, Office of Basic Energy Sciences, under contract ER-46612 for discussions with scientists sponsored by these grants. J.I. acknowledges funding from MINECO-Spain (Grants Nos. MAT2010-18113 and CSD2007-00041).

[1] A. M. Glazer, Acta Crystallogr. Sect. A **31**, 756 (1975).
[2] I. A. Kornev, L. Bellaiche, P. E. Janolin, B. Dkhil, and E. Suard, Phys. Rev. Lett. **97**, 157601 (2006).
[3] M. Fornari and D. J. Singh, Phys. Rev. B **63**, 092101 (2001).
[4] B. Noheda, L. Wu, and Y. Zhu, Phys. Rev. B **66**, 060103(R) (2002).
[5] D. M. Hatch, H. T. Stokes, R. Ranjan, Ragini, S. K. Mishra, D. Pandey, and B. J. Kennedy, Phys. Rev. B **65**, 212101 (2002).
[6] D. I. Woodward, J. Knudsen, and I. M. Reaney, Phys. Rev. B **72**, 104110 (2005).
[7] R. Ranjan, Ragini, S. K. Mishra, D. Pandey, and B. J. Kennedy, Phys. Rev. B **65**, 060102(R) (2002).
[8] D. Vanderbilt and W. Zhong, Ferroelectrics **206**, 181 (1998).
[9] J. C. Wojdeł, P. Hermet, M. P. Ljungberg, P. Ghosez, and J. Íñiguez, J. Phys. Condens. Matt. **25**, 305401 (2013).
[10] D. Sichuga, I. Ponomareva, and L. Bellaiche, Phys. Rev. B **80**, 134116 (2009).
[11] I. C. Infante *et al.*, Phys. Rev. Lett. **105**, 057601 (2010).
[12] D. Sichuga and L. Bellaiche, Phys. Rev. Lett. **106**, 196102 (2011).
[13] B. Houchmandzadeh, J. Lajzerowicz, and E. Salje, J. Phys.: Condens. Matter **3**, 5163 (1991).
[14] H. Liu and B. Dkhil, J. Kristallog. **226**, 163 (2011).
[15] M. E. Lines and A. M. Glass, *Principles and Applications of Ferroelectrics and Related Materials* (Oxford University Press, New York, 1977).
[16] L. Zhu and Q. Wang, Macromolecules **45**, 2937 (2012).
[17] K. M. Rabe, in *Functional Metal Oxides*, edited by S. B. Ogale, T. V. Venkatesan, and M. Blamire (Wiley, New York, 2013); and also available in http://www.physics.rutgers.edu/ karin.
[18] B. Dupé, S. Prosandeev, G. Geneste, B. Dkhil, and L. Bellaiche, Phys. Rev. Lett. **106**, 237601 (2011).
[19] O. Diéguez, O. E. González-Vázquez, Jacek C. Wojdel and J. Íñiguez, Phys. Rev. B **83**, 094105 (2011).

[20]C. J. Howard, R. L. Withers, K. S. Knight, and Z. Zhang, J. Phys.: Condens. Matter **20**, 135202 (2008).
[21]S. Prosandeev, D. Wang, W. Ren, J. Íñiguez and L. Bellaiche, Adv. Funct. Mater. **23**, 234 (2013)
[22]Y. Yang, W. Ren, D. Wang, and L. Bellaiche, Phys. Rev. Lett. **109**, 267602 (2012).
[23]W. Zhong, D. Vanderbilt, and K. M. Rabe, Phys. Rev. Lett. **73**, 1861 (1994); Phys. Rev. B **52**, 6301 (1995).
[24]B. J. Campbell, H. T. Stokes, D. E. Tanner, and D. M. Hatch, J. Appl. Crystallogr. **39**, 607 (2006).
[25]J. Holakovsky, Phys. Status Solidi B **56**, 615 (1973).
[26]I. A. Kornev and L. Bellaiche, Phys. Rev. B **79**, 100105(R) (2009).
[27]E. Salje and M. Carpenter, J. Phys.: Condens. Matter **23**, 462202 (2011).
[28]S. Conti, S. Muller, A. Poliakovsky, and E. Salje, J. Phys.: Condens. Matter **23**, 142203 (2011).
[29]Igor A. Kornev, S. Lisenkov, R. Haumont, B. Dkhil, and L. Bellaiche, Phys. Rev. Lett. **99**, 227602 (2007).
[30]C. J. Howard and H. T. Stokes, Acta Crystallogr. Sect. A **61**, 93 (2005).
[31]E. Bousquet *et al.*, Nature (London) **452**, 732 (2008).
[32]J. M. Rondinelli and C. J. Fennie, Adv. Mater. **24**, 1961 (2012).
[33]J. M. Rondinelli, S. J. May, and J. W. Freeland, MRS Bull. **37**, 261 (2012).